Korean J. Chem. Eng., 33(12), 3407-3416 (2016)
DOI: 10.1007/s11814-016-0195-2

pISSN: 0256-1115
eISSN: 1975-7220

Enhancement of NO absorption in ammonium-based solution using heterogeneous Fenton reaction at low H_2O_2 consumption

Bo Wu, Yuanquan Xiong†, Jinbo Ru, and Hao Feng

Key Laboratory of Energy Thermal Conversion and Control of Ministry of Education, School of Energy and Environment, Southeast University, Nanjing 210096, Jiangsu, China
(*Received 7 February 2016 • accepted 2 July 2016*)

Abstract−A novel NO removal system is designed, where NO is initially oxidized by •OH radicals from the decomposition of hydrogen peroxide (H_2O_2) over hematite and then absorbed by ammonium-based solution. According to the high performance liquid chromatography (HPLC) profile and the isopropanol injection experiments, the •OH radicals are proved to play a critical role in NO removal. The NO removal efficiency primarily depends on H_2O_2 concentration, gas hourly space velocity (GHSV), H_2O_2 feeding rate and reaction temperature, while the flue gas temperature slightly affects the NO removal efficiency. The low H_2O_2 consumption makes this system a promising technique in NO removal process using wet-method. The evolution of catalyst in reaction is analyzed by scanning electron microscopy (SEM), energy dispersive X-ray spectrometry (EDS), Fourier Transform infrared spectroscopy (FTIR) and X-ray diffraction (XRD). The nitrite ion and nitrate ion in aqueous solution are detected by the continuous phase flow analyzer. Finally, the macrokinetic parameters of the NO oxidation are obtained by using the initial rate method.

Keywords: Enhancement of NO Absorption, Heterogeneous Fenton Reaction, Low H_2O_2 Consumption, Hematite, Ammonium-based Aqueous Solution

INTRODUCTION

The emission of SO_2 and NO_x from coal combustion has seriously threatened the human environment [1]. Even though wet flue gas desulfurization (WFGD) and selective catalytic reduction (SCR) have succeeded in SO_2 removal and NO removal, respectively, these approaches need excessive setups to remove multiple pollutants, thereby leading to the large occupation and high investment. Several multiple pollutant removal methods, such as plasma removal, activated carbon adsorption and liquid absorption, have been proposed and reported recently [2-9]. The majority of these investigations focus on the liquid absorption process due to its feasibility in conventional WFGD scrubbers. The demerit of liquid absorption is low NO removal efficiency, mainly because the major NO_x component (over 90%) in flue gas is sparingly soluble NO. Compared with NO, the high valence NO_x such as NO_2 or N_2O_3 can be easily absorbed by liquid phase due to its high solubility in aqueous solution. Hence, various oxidants (e.g., $NaClO_2$ or $KMnO_4$) as additives have been tested and the enhancement effects performed in previous reports [10-14]. However, these oxidants and byproducts bring large quantities of wastewater, which is also a kind of secondary pollutant. H_2O_2 is a kind of green chemical oxidant that decomposes into water and oxygen finally, but its oxidation capacity is weak when the H_2O_2 concentration is lower than 70 wt% [15].

Compared to H_2O_2, the •OH radicals from the H_2O_2 decomposition show higher reactive, which can decrease the contamination concentration in wastewater from several-hundreds ppm to less than 5 ppb. However, the decomposition rate of H_2O_2 in aqueous solution without catalyst is slow. Ultraviolet, ultrasonic and transition metal oxides catalysts are often used to accelerate the decomposition of H_2O_2 into •OH radicals. Among them, the heterogeneous Fenton reaction using transition metal oxides catalysts is an efficient approach to generate •OH radicals in even room temperature [16]. Compared with the homogeneous Fenton reaction, the heterogeneous Fenton reaction has great advantages, such as avoiding iron sludge generation, easy recycling and regeneration of catalyst, low energy consumption and simple operation [17]. Hence, the heterogeneous Fenton reaction has great application potential in environmental protection technology.

The •OH radicals could react with NO immediately due to the high standard electrode potentials (+2.8 eV). The oxidation products, such as NO_2 or nitrite acid, could be easily absorbed by the ammonium-based solution. The operation condition in the flue gas field is totally different from aqueous solution such as high flue gas temperature (over 140 °C) and large flue gas flow rate (usually 4,000 Nm^3 per MW). The high flue gas temperature could accelerate the self-decomposition of H_2O_2 and generated O_2. The large flue gas flow rate might bring a large consumption of H_2O_2. The two aspects might cause a large consumption of H_2O_2 and, consequently, increase the operation cost. Qin proposed a simultaneous NO_x and SO_2 removal process that combined ammonia desulfurization technique with heterogeneous Fenton reaction [18-21]. According to his proposal, •OH radicals are generated from the catalytic decomposition of H_2O_2 over hematite in the catalytic reactor and then injected into flue gas. The pre-oxidized flue gas is absorbed by

†To whom correspondence should be addressed.
E-mail: yqxiong@seu.edu.cn
Copyright by The Korean Institute of Chemical Engineers.

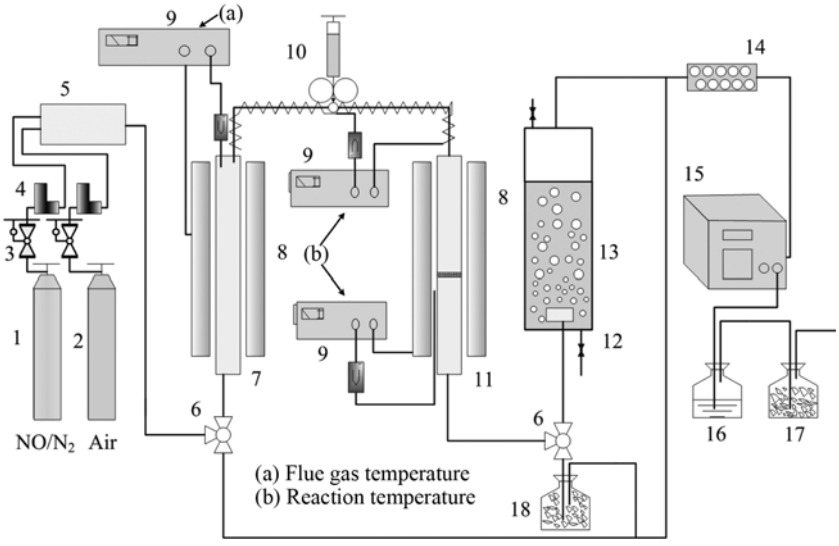

Fig. 1. Schematic diagram of the experimental apparatus.

1. NO/N_2	6. Tee valve	11. Catalytic reactor	16. $KMnO_4$/NaOH solution
2. Air	7. Preheater	12. Distributor	17. Activated carbon
3. Valve	8. Heater	13. Bubbling reactor	18. $Ca(OH)_2$
4. Mass flow controller	9. Temperature control unit	14. Anhydrous calcium chloride	
5. Buffer	10. Syringe pump	15. Flue gas analyzer	

ammonia-based absorbent. In his bench scale device, about 80% NO is removed from the inlet simulated flue gas (240 mL/min, 500 ppm NO included) when the feeding rate of 30 wt% H_2O_2 is about 0.4 mL/min. The molar ratio of oxidation to NO in a unit time is about 738 times. The excessive H_2O_2 consumption means high operation cost. Liu et al. focus on the UV/Fenton reaction in the SO_2 and NO removal process [4,22-24]. About 72% NO removal efficiency is achieved in the bubbling bed when the UV lamp power is more than 36 W. However, NO and SO_2 could only react with the •OH radicals in the liquid-gas interface and •OH radicals might annihilate in the bulk. It is hard to figure out the utilization of H_2O_2 in a bubbling bed and control the consumption of H_2O_2. As far as we know, few papers have reported the high efficient NO removal from flue gas by heterogeneous Fenton reaction with controllable and low H_2O_2 consumption.

In this paper, a novel system is designed to enhance the NO absorption in ammonium-based aqueous solution by heterogeneous Fenton with low H_2O_2 consumption. The critical role of •OH radicals in the NO removal is determined by HPLC and isopropanol injection experiments. The main parameters like H_2O_2 concentration, H_2O_2 feeding rate, GHSV, reaction temperature, are intensively discussed. What's more, the characters of catalyst before and after reaction are analyzed by FTIR spectrometer, SEM-EDX and XRD pattern. The nitrite ion and nitrate ion in solution is analyzed by continuous phase flow analyzer. Finally, the reaction mechanism is speculated by the experimental results, and macrokinetics parameters are obtained using initial rate method.

EXPERIMENTAL SECTION

1. Catalyst Synthesis

The Fe_2O_3 catalyst was prepared by the conventional Pechini method. Aqueous precursor solutions were prepared by dissolving $Fe(NO_3)_3 \cdot 9H_2O$ (≥99.0 wt%, analytically pure, Ningshi Chemical Reagent Company, Nanjing, China), citric acid (≥99.5 wt%, analytically pure, Ningshi Chemical Reagent Company, Nanjing, China) and PEG-400 (Mn=400, Aladdin) into 40 mL reverse osmosis water. The precursor solutions were heat-treated at 80 °C for 5 hours to obtain hard gel. Then, the hard gel was first dried in 100 °C for 10 hours and then was calcinated at 500 °C for 5 hours.

2. Experimental Procedure

The experimental system is shown in Fig. 1. Air and NO/N_2 (Nanjing MaikesiNanfen Special Gas Co., Ltd.) in cylinders was supplied from cylinders to simulate the main components in practical flue gas. The gas flow rate was regulated by mass flow controller (MFC, Beijing Sevenstar Electronics Co., Ltd.). The simulated flue gas was mixed well in the buffer and then preheated. The H_2O_2 (30.0 wt%, analytically pure, United Initiators (Shanghai) Co., Ltd.) was injected into the pipe by syringe pump (BYZ-810, Changsha Beyond Medical Devices Co., Ltd.) and heated by the simulated flue gas and pipe. In a small H_2O_2 feeding rate, the H_2O_2 was vaporized and purged with by the simulated flue gas. The blended gas flowed through the catalytic reactor where H_2O_2 decomposed over the hematite and generated •OH radicals. The oxidation of NO also proceeded to completion in this area. Then the flue gas reacted with the absorbent in the glass-made bubbling reactor (Height, 600 mm; Inside diameter, 50 mm). Before the experiments began, the reactor was filled with ammonium-based absorbent solution. The volume of absorbent solution was 1 L (about 0.51 m liquid height) at any operation conditions. The ammonium-based aqueous solution used in this paper proved to be a kind of effective absorbent for NO_x [25]. The ammonium-based absorbent consisted of 5 wt% urea (≥99.0 wt%, analytically pure, Ningshi Chemical Reagent Company, Nanjing, China), 5 wt% ammonium sulfite (25-

28 wt%, analytically pure, Shanghai Jiuyi chemical reagent Co., Ltd.) and 0.015 wt% triethanolamine (≥92.0 wt%, analytically pure, United Initiators (Shanghai) Co., Ltd.). The temperature control unit consisted of a PID temperature controller and thermal resistance (WZP-PT100, uncertainty=±1 °C, −20 °C~200 °C). The reactor temperature was showed in the temperature transmitter. The gas products in the outlet were read out from the flue gas analyzer (pFLUE2000, 0-2,000 ppm, accuracy=±2% rel., repeatability=±1% rel. for NO, BigDipper Technochem Institute, Beijing, China) to detect the dry concentration value of different components. The NO concentration was calibrated with 800 ppm NO before each run. The calculation method of NO removal efficiency is shown in Eq. (1):

$$E_N = \frac{c_i(NO) - c_o(NO)}{c_i(NO)} \quad (1)$$

where E_N represents the NO removal efficiency (%); c_i and c_o represents the NO concentrations (ppm) at the inlet and the outlet of the scrubber, respectively. The NO concentration was measured by flue gas analyzer before and after reaction and all the data were recorded for 3 min until a steady-state operation was maintained.

The continuous phase flow analyzer (Skalar San plus System, Dutch) was used to measure the concentrations of NO_2^- and NO_3^-. FTIR spectra were recorded on a Bruker Vector22 FTIR spectrometer. Microstructures of the catalyst before and after reaction were analyzed by an SEM (LEO 1530 VP) equipped with an EDS analytical system. The XRD patterns of catalyst before and after reaction were recorded on a Rigaku D/max 2500 PC X-Ray diffractometer with a CuKα radiation (λ=0.15406 nm) using a tube voltage of 40 kV and current of 100 mA. The 2θ ranged from 5° to 85° and was measured in steps of 10°/min.

The •OH radicals were detected by HPLC (Agilent, USA) using salicylic acid (≥99.0 wt%, analytically pure, Ningshi Chemical Reagent Company, Nanjing, China) as the molecule probe. A complex aqueous solution including salicylic acid, catalyst and H_2O_2 was kept for 1 hour in the dark at 20 °C. The procedure of isopropanol injection experiments was shows as follows. The H_2O_2 prepared by water or isopropanol (≥99.5 wt%, analytically pure, Ningshi Chemical Reagent Company, Nanjing, China) was injected into the reactor to figure out the effect of •OH radicals on NO oxidation.

The macrokinetics of NO oxidation was studied using initial rate method. Before experiments began, the simulated flue gas was switched into $Ca(OH)_2$ (≥99.0 wt%, analytically pure, Ningshi Chemical Reagent Company, Nanjing, China) rather than bubbling reactor. The high valence NO_x, nitrite acid and nitrate acid were absorbed by $Ca(OH)_2$ and NO was detected by the flue gas analyzer.

RESULTS AND DISCUSSION

1. Effect of Catalyst and H_2O_2 on NO Removal

The NO removal efficiencies in different reaction systems are shown in Table 1. Test 1 was the blank test to evaluate the NO removal efficiency using ammonium-based absorbent only. Tests 2-7 were conducted using H_2O_2 solution without hematite catalyst added. From the experimental results, the ammonium-based absorbent had little NO removal efficiency, which was about 27%. The highest NO removal efficiency among tests 2-7 was 50.3% when the H_2O_2 concentration was 10 mol/L. However, H_2O_2 showed no obvious effect on the NO removal process when the H_2O_2 concentration was below 2 mol/L. Tests 8-10 were conducted to test the performance of hematite without H_2O_2 injection. It was indicated that the hematite could not enhance the NO removal efficiency. Tests 11 and 12 were carried with H_2O_2 (2 mol/L and 5 mol/L) and hematite (2 g), where the NO removal efficiencies were 78% and 91.5%, respectively. The results showed that H_2O_2 was the reactant in the experimental process and the hematite could enhance the oxidation ability of H_2O_2. The enhancement mechanism of hematite on H_2O_2 was related to the •OH radicals generation over the catalyst. According to the Haber-Weiss mechanism, the decomposition of H_2O_2 over hematite could be presented as reactions (2)-(5) [26-28]:

Table 1. The comparison of NO removal efficiency under different operation condition

Test	H_2O_2 concentration mol/L	H_2O_2 feeding rate mL/h	Fe_2O_3 (g)	NO removal efficiency (%)
1	0	0	0	27.0
2	1	5	0	27.5
3	2	5	0	28.8
4	4	5	0	36.3
5	6	5	0	41.4
6	8	5	0	48.0
7	10	5	0	50.3
8	0	0	0.6	27.2
9	0	0	1	27.5
10	0	0	2	27.8
11	2	5	2	78.0
12	5	5	2	91.5

Operation condition: gas flow rate: 1.5 L/min, C(NO)=530 ppm, $C(O_2)$=7%, flue gas temperature: 140 °C, reaction temperature: 140 °C

$$\equiv Fe(III) + H_2O_2 \rightarrow \equiv Fe(II) + HO_2^{\bullet}(O_2^{\bullet}) + H^+(2H^+) \quad (2)$$

$$HO_2^{\bullet} \leftrightarrow O_2^{\bullet -} + H^+ \quad (3)$$

$$\equiv Fe(III) + HO_2^{\bullet} \rightarrow \equiv Fe(II) + O_2(+H^+) \quad (4)$$

$$\equiv Fe(II) + H_2O_2 \rightarrow \equiv Fe(III) + {}^{\bullet}OH + OH^- \quad (5)$$

In this work, the formation of •OH radicals over the catalyst was proved by HPLC method. The salicylic acid as molecular probe could react with •OH radicals, producing 2, 3-dihdroxybenzoic acid (2, 3-DHBA) and 2, 5-dihdroxybenzoic acid (2, 5-DHBA) [29]. The production could be detected by HPLC analysis and, thereby, the •OH radicals formation could be proved. From Fig. S1, both 2, 3-DHBA and 2, 5-DHBA were not found in the pure H_2O_2 sample, while they were detected in the H_2O_2/Fe_2O_3 sample. The results indicated that a great amount of •OH radicals could be produced by decomposition of H_2O_2 over catalyst in relatively short time. Further, H_2O_2/isopropanol and H_2O_2/water was injected into catalytic reactor, respectively. From Fig. S2, the NO removal effi-

ciency using H_2O_2/isopropanol was much lower than that using H_2O_2/water and even similar to the blank test. As is known, isopropanol is often used as a kind of typical radical annihilation. The comparison indicated that the •OH radicals played a critical role in NO removal.

In consideration of economic factors, this enhancement effect of hematite on the catalytic decomposition of H_2O_2 also facilitated the application of this technical in the practical. From Table 1, the NO removal efficiency under 2 mol/L H_2O_2 feeding rate was about 78% with the catalyst added. Under this condition, the molar consumption of oxidant was five-times that of NO. When the catalyst was 0 g, the highest efficiency (50.3%) was observed using 10 mol/L H_2O_2 concentrations. The molar consumption of oxidant was 25-times that of NO. Thus the additive catalyst was in favor of decreasing H_2O_2 consumption. Besides, the hematite was easlyy handled, relatively low cost and environmental benign character. In summary, the proposed approach has the advantages of feasibility and low cost, which could be able to fulfill its industrial application.

2. Effect of H_2O_2 Concentration on NO Removal

To investigate the effect of H_2O_2 concentration on NO removal, a series of experiments with H_2O_2 concentrations in the range of 1 mol/L H_2O_2 (about 3 wt%) to 10 mol/L H_2O_2 (about 30 wt%) were performed. Curves in Fig. 2 show that H_2O_2 concentration was one of the key factors in NO removal. The NO removal efficiency was about 78% when the H_2O_2 concentration was 2 mol/L. Further increment on the H_2O_2 concentration could enhance the NO removal efficiency to a large extent. The reason could be explained as follows. On one hand, the increased H_2O_2 concentration could enhance the shift of reactions (2)-(5) and, consequently, promote the production of •OH radicals on the catalyst surface. The incremental •OH radicals facilitated the oxidation of NO, leading to a high absorption efficiency in liquid phase. On the other hand, •OH radicals could desorb from the catalyst surface and diffuse to gas phase. The diffusion rate was proportional to the different •OH radicals concentration between gas phase and the catalyst surface.

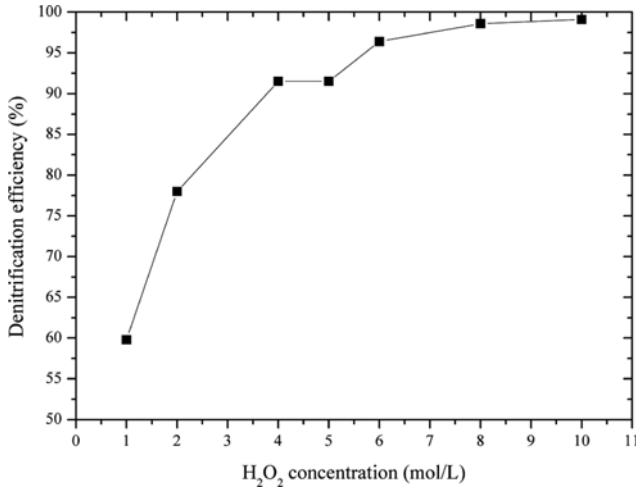

Fig. 2. Effect of H_2O_2 concentration on NO removal efficiency. Condition: gas flow rate: 1.5 L/min, C(NO)=530 ppm, C(O_2)=7%, flue gas temperature: 140 °C, reaction temperature: 140 °C, H_2O_2 feeding rate: 5 mL/h, GHSV: 45,000 h^{-1}.

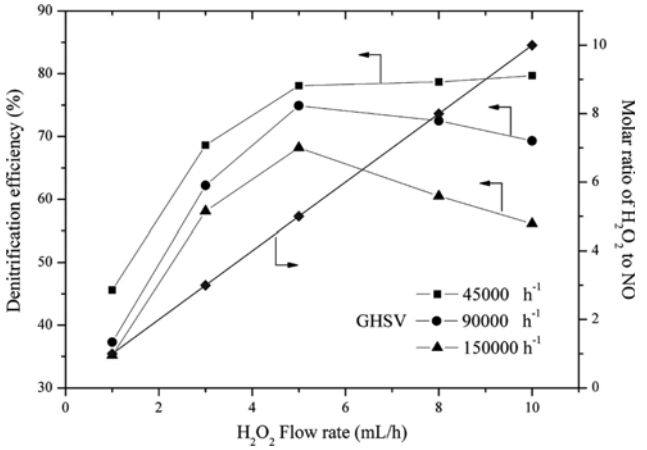

Fig. 3. Effect of GHSV and H_2O_2 feeding rate on NO removal efficiency. Condition: gas flow rate: 1.5 L/min, C(NO)=530 ppm, C(O_2)=7%, flue gas temperature: 140 °C, reaction temperature: 140 °C, H_2O_2 concentration: 2 mol/L.

The incremental H_2O_2 concentration facilitated the generation of •OH radicals and, consequently, promoted the diffusion from the catalyst surface to the gas phase. Products like NO_2 or nitrite acid in the gas phase were more easily removed by flue gas than in the pore of catalyst. Thus, the incremental H_2O_2 concentration could dramatically increase NO removal efficiency.

Even though the usage of high concentration H_2O_2 could achieve a high NO removal efficiency, the safety in store is a big question in practical engineering. Hence, in consideration of both NO removal efficiency and safety, 2 mol/L was selected as the optimal H_2O_2 concentration.

3. Effect of GHSV and H_2O_2 Feeding Rate on NO Removal

GHSV is an important index in the solid-gas catalytic process. The GHSV indicates how many reactor volumes of feed can be treated using a unit volume of catalyst in a unit time. The influence of GHSV on the NO removal is shown in Fig. 3. When H_2O_2 feeding rate remained at 5 mL/h, the NO removal efficiency decreased rapidly from 78% to 65% with the GHSV increasing from 45,000 h^{-1} to 150,000 h^{-1}. The low GHSV value meant the high usage of catalyst in the catalytic reactor. At low GHSV, both the contact area between H_2O_2 and catalyst and the residual time of H_2O_2 in the catalytic area increased, leading to the incremental •OH radicals. The more •OH radicals were produced the more completely NO molecules in the flue gas were oxidized. It is widely known that the mass transfer rate of high valence NO_x in aqueous solution is obviously higher than NO. Thus the decrease of GHSV is conducive to the absorption of NO_x in our experimental system.

The influence of H_2O_2 feeding rate on NO removal represents the molar ratio of H_2O_2 to NO, which is proportional to the economic factor as a significant index. Hence, the investigation on H_2O_2 feeding rate has important engineering meaning. The results are shown in Fig. 3. In a certain GHSV, for example at 45,000 h^{-1}, the NO removal efficiency increased from 45% to about 79% when the H_2O_2 feeding rate increased from 1 mL/h to 10 mL/h. In theory, the increased H_2O_2 feeding rate meant that the molar weight of H_2O_2 in the flue gas increased, which would promote the diffu-

sion of H_2O_2 from the gas to the catalyst. Therefore, the increased H_2O_2 feeding rate would facilitate the production of •OH, leading to an incremental NO removal efficiency. However, experimental results showed the opposite phenomenon, especially at the high GHSV. When the GHSV was 150,000 h^{-1}, the NO removal efficiency increased with the H_2O_2 feeding rate increased in the range of 1 mL/h-5 mL/h and began to decrease with the H_2O_2 increased in the range of 5 mL/h-10 mL/h. The reasons could be as follows. The increased H_2O_2 feeding rate means that more H_2O_2 solution was injected into the catalytic reactor. It is difficult to vaporize such large amount of H_2O_2 solution completely in a relatively short time. H_2O_2 or H_2O might condense into little liquid drop and some •OH radicals are dissolved in the liquid drop. Under this condition, •OH radicals would disperse badly in simulated flue gas, which could weaken the oxidation ability of •OH radicals. Further, side reactions (6) and (7) occur and the H_2O_2 could also be the terminator of •OH radicals. The oxidation capacities of H_2O_2 (+1.77 eV) and HO_2• radicals (+1.60 eV) are much weaker than that of •OH radicals (+2.80 eV). Therefore, further increase of H_2O_2 feeding rate leads to the constant or decline of NO removal efficiency. The optimal H_2O_2 feeding rate among the investigated operation condition is 5 mL/h.

$$\cdot OH + \cdot OH \rightarrow H_2O_2 \quad (6)$$

$$\cdot OH + H_2O_2 \rightarrow HO_2^{\cdot} + H_2O \quad (7)$$

4. Effect of Temperature on NO Removal

The reaction temperature was an important factor in the H_2O_2 decomposition and NO oxidation. From Fig. 4(a), the increment of reaction temperature improved the NO removal efficiency from about 70% to 82% when the temperature ranged from 120 °C to 160 °C. The reasons might be threefold. First, the reaction temperature affected the decomposition of H_2O_2 rate by a big margin. According to the Arrhenius, the decomposition rate of H_2O_2 was mainly related with the reaction temperature showed as Eq. (8):

$$k = Ae^{-E/RT} \quad (8)$$

where A is the pre-exponential factor; E is the apparent activation energy, kJ/mol; R is the universal gas constant, 8.314 $J \cdot mol^{-1} \cdot K^{-1}$; and T is the absolute temperature, K.

The rate constant of a chemical reaction (k) depended on the pre-exponential factor (A), the activation energy (E), the reaction temperature (T) and the universal gas constant (R). From Eq. (8), the rate constant of a chemical reaction (k) increased with the reaction temperature (T) increased when other factors kept constant. It was indicated that, with the reaction temperature increased, the decomposition rate of H_2O_2 could be accelerated, which had a positive effect on the •OH radicals production. Due to the key role of •OH radicals on the NO oxidation, the NO removal efficiency could be enhanced. Second, with the reaction temperature increased, the kinetic energy of adsorptive •OH radicals was enhanced and the •OH radicals tended to be desorbed from the catalyst surface. Hence, the incremental temperature might be conducive to the diffusion of •OH radicals from catalyst surface to the gas phase. Accordingly, •OH radicals had a good dispersion in the simulated flue gas and accelerated the oxidation reaction in the gas phase. Third, as the boiling point of H_2O_2 aqueous solution was over 100 °C, H_2O_2 in gas phase would condense and form liquid droplet on the catalyst surface at low temperature. The droplet would dissolve many •OH radicals and, consequently, the decreasing •OH radicals weakened the oxidation of NO in gas phase. Thus, the NO removal efficiency decreased with the reaction temperature decreased. Because 140 °C is usually considered as a typical reaction temperature in low temperature SCR, it was selected to finish other parts of this research.

The flue gas temperature was measured at the outlet of the preheater. From Fig. 4(b), the flue gas temperature had no obvious effect on NO removal. It was mainly decided by the oxidation mechanism in the system. Compared with the conventional selective catalytic oxidation, the oxidation in this system was from the decomposition of H_2O_2 over the catalyst. Accordingly, the adsorption of NO on the catalyst was not important, while the diffusion of •OH radicals was significant. When the reaction temperature did not change, the reaction rate remained constant and the flue gas temperature had no obvious influence on the H_2O_2 decomposition. However, the flue gas temperature might affect the diffu-

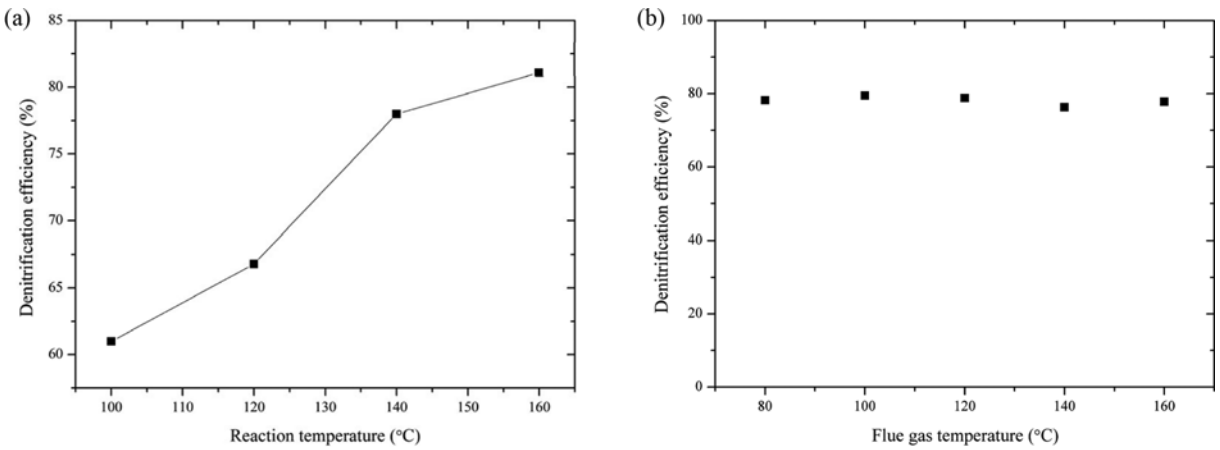

Fig. 4. Effect of temperature on NO removal efficiency. Condition: gas flow rate: 1.5 L/min, C(NO)=530 ppm, C(O_2)=7%, GHSV: 45,000 h^{-1}, H_2O_2 concentration 2 mol/L, H_2O_2 feeding rate: 5 mL/h. (a) Reaction temperature; (b) flue gas temperature.

sion of H_2O_2 vapor and the flow distribution in the large-scale device, and the relevant researches would be made in the future.

5. Under Optimal Parameters for NO Removal

Based on the above analysis, the optimal operation conditions of the experiments were established, where the gas flow rate was 1.5 L/min, flue temperature was 140 °C, reaction temperature was 140 °C, H_2O_2 concentration was 2 moL/L, H_2O_2 feeding rate was 5 mL/h, GHSV was 45,000 h^{-1}. To investigate the change of catalyst and absorbent aqueous solution, a relatively long-time run was carried out and the NO concentration was recorded for every 15 min. The calculated NO removal efficiency is shown in Fig. 5.

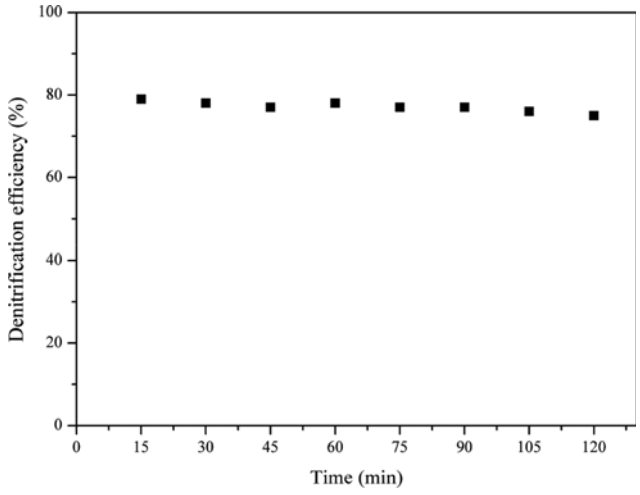

Fig. 5. NO removal efficiency in 2 hours under optimal operation condition. Conditions: gas flow rate: 1.5 L/min, C(NO)=530 ppm, C(O_2)=7%, flue gas temperature: 140 °C, reaction temperature: 140 °C, H_2O_2 concentration: 2 moL/L, H_2O_2 feeding rate: 5 mL/h, GHSV: 45,000 h^{-1}.

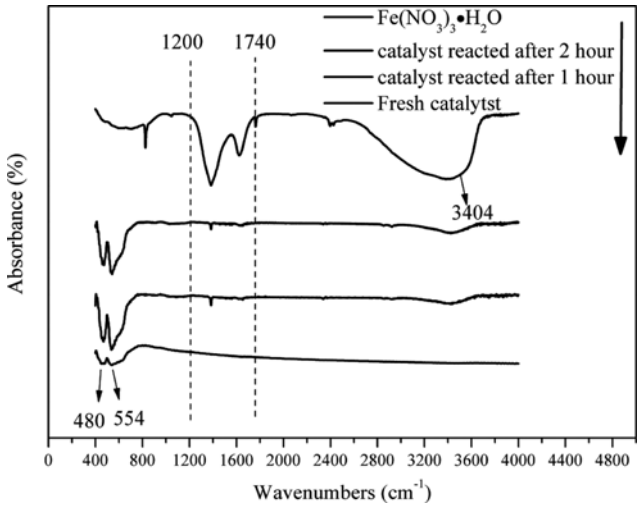

Fig. 6. FTIR spectra of catalyst before and after reaction.

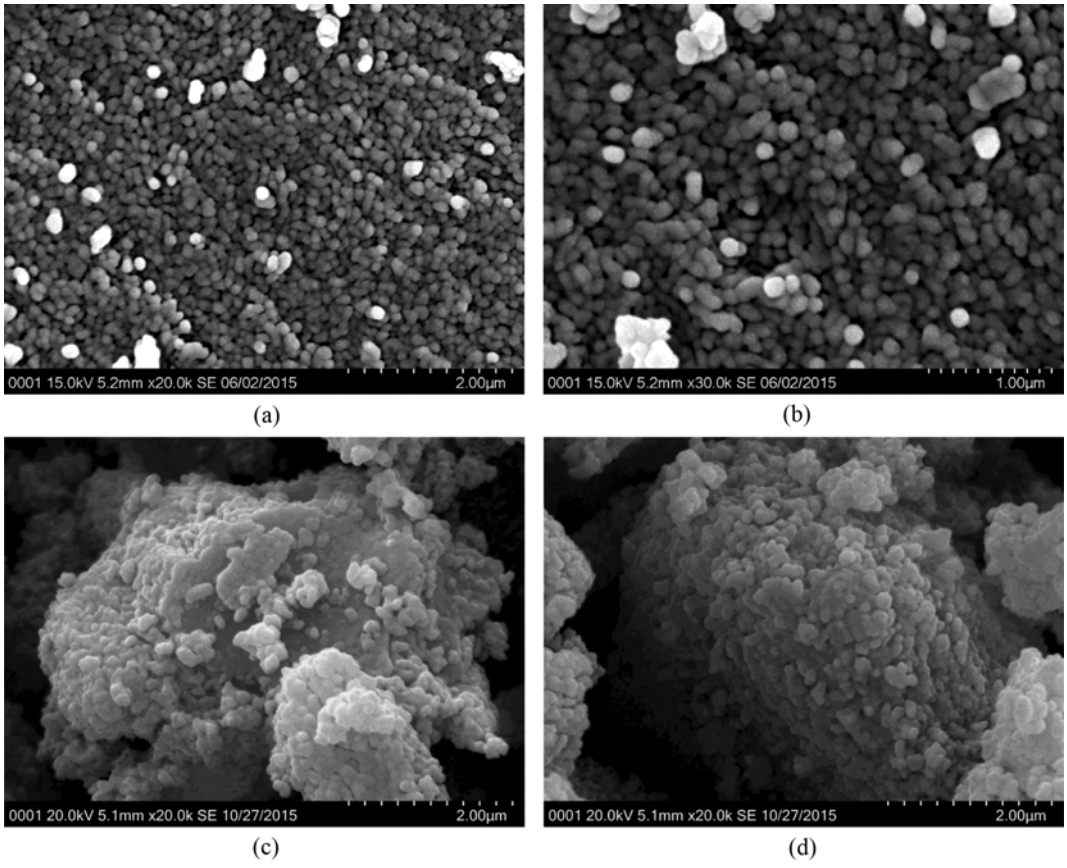

Fig. 7. SEM images of samples (a), (b) fresh catalytic; (c) reaction after 1 h; (d) reaction after 2 h.

The trend remained relatively stable and showed a little declination when the experiment lasted out for two hours. The NO removal efficiency was about 77% when the concentrations of O_2 and NO were 7% and 530 ppm, respectively. When the experiment was carried out for 1 hour and 2 hours, a slight amount of catalyst sample and liquid samples was taken for further analysis, respectively.

6. FTIR Spectra of Catalyst Before and After Reaction

Curves in Fig. 6 present a comparison of FTIR spectra between fresh samples, the reacted sample, and the $Fe(NO_3)_3{\cdot}9H_2O$ sample. Note that the bands of catalyst after reaction had a slight change in the range of 1,200-1,740 cm^{-1} and 3,200-3,400 cm^{-1}. According to previous reports, the 480 and 554 cm^{-1} bands were attributed to the dipole moments in hematite [30,31]. The bands located at 601, 876 and 1,051 cm^{-1} may be ascribed to FeOH and OOH bending vibrations in amorphous FeOOH [32]. The band in the range 1,200-1,740 cm^{-1} was assigned to nitrate ion (NO_3^-) [33]. The band located at 3,404 cm^{-1} was due to OH stretching vibrations of adsorbed H_2O [18]. Hence, the main change of catalyst after reaction could be ascribed to the formation of the ferric nitrate due to the reaction between nitrate acid mist in the gas phase and hematite. The formation of ferric nitrate might be a possible reason for the declination of NO removal efficiency.

7. SEM-EDX Analysis

From Fig. 7, SEM inspection shows that fresh catalyst was mainly constituted of pellet-type hematite (Fig. 7(a) and Fig. 7(b)). Each particle was about 100-200 nm. But some large, smooth and pellet-type morphology was also observed in the samples due to the grain growth in the calcinations (Fig. 7(b)). After experiments were carried out for 1 hour, the particles in the sample tended to aggregate together and formed lamellar-structure hematite (Fig. 7(c)). The image of the sample in Fig. 7(d) presented that the lamellar-structure hematite was further aggregated after 2 hours' reaction and formed a bulk block. The reason was mainly contributed to the nano-scale catalyst particles. In the typical catalytic reaction, catalyst in nano-scale tended to rapidly aggregate and produce large clusters, which led to the reduction of the active surface area [34].

The EDX profiles provided relative amounts of atoms like Fe, O and N in catalyst before and after reaction. From Table 2, the fresh catalyst contained Fe and O only. After 1 hour's reaction, the nitrogen element was found in the sample. The nitrogen atomic percent was about 3% after 1 hour's reaction and the nitrogen element on the sample almost remained constant when the experiments proceeded for 2 hours. The EDX result was in accordance with FTIR spectra. It was implied that the content of $Fe(NO_3)_3$ in catalyst could be negligible in 2 hours' experiments. Accordingly, the nitrate acid mist was mainly absorbed by the liquid absorbent and, hence, the nitrate nitrogen element balance in NO removal could be calculated based on results mentioned above.

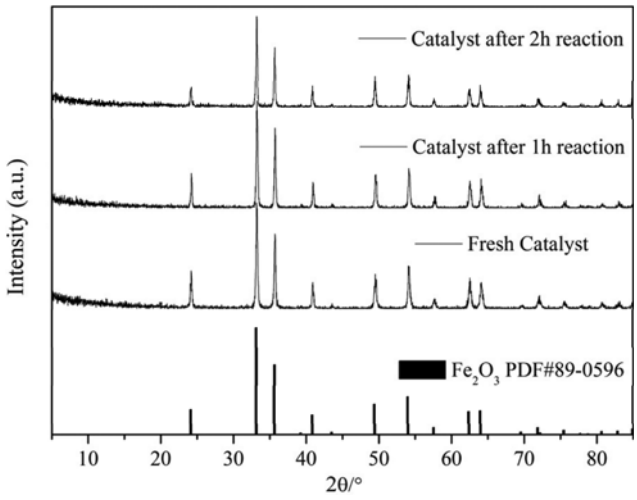

Fig. 8. XRD pattern of catalyst before and after reaction.

8. XRD Analysis

Fig. 8 shows the XRD spectra of fresh catalyst, catalyst after 1 hour's reaction and catalyst after 2 hours' reaction. The diffraction peaks of fresh catalyst corresponding to hematite (PDF#89-0596) appea in XRD patterns. According to the XRD pattern, the structure of catalyst did not change obviously and only hematite was found in the XRD pattern. What's more, $Fe(NO_3)_3$ was not found in the XRD pattern of catalyst after reaction. The reason might be ascribed to the low concentration of $Fe(NO_3)_3$ which was lower than the detection limitation of XRD analyzer (about 1%) and, consequently, hardly detected by XRD. It was also proved by the EDS profile in Table 2 where the N atomic percentage was about 3% even though the reaction was carried out for 2 hours. The above analysis indicated that the Fe_2O_3 catalyst was structurally robust in the 2 hours' reaction.

9. Analysis of Ion Products in Aqueous Solution

The experiments at optimal operation condition were carried out for 60 min and 120 min. The calculation results are shown in Table 3. The major nitrate nitrogen product in aqueous solution was nitrate ion whose concentration was 19.811 mg/L at 60 min and 48.004 mg/L at 120 min. The minor nitrate nitrogen product was nitrite ion whose concentration was 1.730 mg/L at 60 min and 5.817 mg/L at 120 min. To make evolution of the nitrate nitrogen in NO removal system clear, a calculation was made as follows.

Table 2. EDS analysis of catalyst before and after reaction

Element	Fresh catalyst		After 1 hour's Reaction		After 2 hours' Reaction	
	Atomic percent	Atomic percent error	Atomic percent	Atomic percent error	Atomic percent	Atomic percent error
O	59.69	+/−6.29	53.82	+/−6.29	58.21	+/−6.85
Fe	40.31	+/−7.03	43.17	+/−7.00	38.87	+/−6.91
N			3.01	+/−0.77	2.92	+/−0.24
Total	100.00		100.00		100.00	

Table 3. Analysis of nitrate nitrogen in NO removal

Category	Initial absorbent	Run 1	Run 2
Time t, min	0	60	120
Gas flow rate Q, L/min	-	1.5	1.5
Solution volume V, L	1	1	1
C_{in}(NO), ppm	-	530	530
C_{out}(NO), ppm	-	116.6	132.5
Denitrification efficiency	-	78%	75%
$C(NO_2^-)^{actual}$, mg/L	0	1.730	5.817
$C(NO_3^-)^{actual}$, mg/L	0	19.811	48.004
$n(NO_2^-)^{actual}$, mmol	0	0.038	0.126
$n(NO_3^-)^{actual}$, mmol	0	0.320	0.774
$n(N)^{actual}$, mmol	0	0.358	0.900
$n(N)^{calculation}$, mmol	0	1.661	3.194
$n(N)^{error}$, mmol	0	1.341	2.420

Operation condition: gas flow rate: 1.5 L/min, C(NO)=530 ppm, $C(O_2)$=7%, flue gas temperature: 140 °C, reaction temperature: 140 °C

The actual molar weight of nitrate ion or nitrite ion could be calculated as Eqs. (9)-(10):

$$n(NO_2^-)^{actual}=\frac{V*C(NO_2^-)^{actual}}{M(NO_2^-)} \quad (9)$$

$$n(NO_3^-)^{actual}=\frac{V*C(NO_3^-)^{actual}}{M(NO_3^-)} \quad (10)$$

where n is the molar weight of nitrite ion and nitrate ion (mmol); V is the solution volume (L); C is the ion concentration in aqueous solution (mg/L); M is the molar mass (g/mol).

The sum of $n(NO_2^-)^{actual}$ and $n(NO_3^-)^{actual}$ was calculated by Eq. (11)

$$n(N)^{actual}=n(NO_3^-)^{actual}+n(NO_2^-)^{actual} \quad (11)$$

where $n(N)^{actual}$ was the sum of $n(NO_2^-)^{actual}$ and $n(NO_3^-)^{actual}$ in the aqueous solution (mmol).

Based on the nitrogen element balance in the whole reaction process, the difference between $n(N)^{calculation}$ and $n(N)^{actual}$ was calculated as Eq. (12):

$$n(N)^{error}=n(N)^{calculation}-n(N)^{actual} \quad (12)$$

where the $n(N)^{calculation}$ was calculated as the method proposed by Liu [4,22] (mmol), $n(N)^{error}$ was the difference between $n(N)^{calculation}$ and $n(N)^{actual}$ (mmol).

The $n(N)^{error}$ might be from two aspects: the experimental error and the reduction of nitrite acid by urea and ammonium sulfite in the aqueous solution. The $n(N)^{error}$ for 60 min and 120 min was 1.341 mmol and 2.420 mmol, respectively, while the $n(N)^{calculation}$ for 60 min and 120 min was 1.661 mmol and 3.194 mmol, respectively. According to Liu's reports [4,22], this method usually cannot result in such a big error. A plausible explanation was that the $n(N)^{error}$ was mainly from the latter. The reduction of nitrite acid by urea and ammonium sulfite produced nitrogen, and the nitrogen gas could not be detected by our flue gas analyzer. Hence this part of nitrogen could not be calculated and resulted into the $n(N)^{error}$.

REACTION MECHANISM AND MACROKINETICS

1. Reaction Mechanism

On the basis of our experimental results, it was common sense that the high oxidizing ability of •OH radicals played the main role in the oxidation of NO. In the whole NO removal system, the possible major reactions were listed as follows:

First, the production of •OH radicals in the catalytic reactor was mentioned above showed in reactions (2)-(5);

Second, the oxidation of NO in the whole reactor is shown in reactions (13)-(17) [19,35]:

$$NO+{}^{\bullet}OH\rightarrow HNO_2 \quad (13)$$

$$NO+{}^{\bullet}OH\rightarrow NO_2+{}^{\bullet}H \quad (14)$$

$$NO_2+{}^{\bullet}OH\rightarrow HNO_3 \quad (15)$$

$$NO_2^-+{}^{\bullet}OH\rightarrow NO_3^-+H^+ \quad (16)$$

$$2NO+3H_2O_2\rightarrow 2HNO_3+2H_2O \quad (17)$$

Third, the reaction between nitrate acid vapor and hematite is shown in reaction (18):

$$6HNO_3+Fe_2O_3\rightarrow 2Fe(NO_3)_3+3H_2O \quad (18)$$

Fourth, the oxidation and absorption of NO in the scrubber:

The oxidation of NO in the scrubber is shown in reactions (19)-(20) [36]:

$$2NO+3H_2O_2\rightarrow 2NO_3^-+2H^++2H_2O \quad (19)$$

$$NO_2^-+H_2O_2\rightarrow NO_3^-+H_2O \quad (20)$$

The reduction of NO_x in the scrubber showed in reactions (21)-(24) [19,37,38]:

$$NO+NO_2+CO(NH_2)_2\rightarrow 2N_2=CO_2+2H_2O \quad (21)$$

$$2(NH_4)_2SO_3+2NO\rightarrow 2(NH_4)_2SO_4+N_2 \quad (22)$$

$$(NH_4)_2SO_3+2NO_2+H_2O\rightarrow (NH_4)_2SO_4+2HNO_2 \quad (23)$$

$$3(NH_4)_2SO_3+2HNO_2\rightarrow 3(NH_4)_2SO_4+N_2+H_2O \quad (24)$$

The reaction between triethanolamine and N_2O_4 is shown in reactions (25)-(26) [25]:

$$2N(CH_2CH_2OH)_3+N_2O_4\rightarrow[N(CH_2CH_2OH_3]_2\cdot N_2O_4 \rightarrow[N(CH_2CH_3OH)_3\cdot NO]^+NO_3^- \quad (25)$$

$$[N(CH_2CH_3OH)_3\cdot NO]^+NO_3^-+N_2O \rightarrow(CH_2CH_3OH)_3NH^+NO_3^-+(CH_2CH_3OH)_3NH^+NO_2^- \quad (26)$$

2. Macrokinetics of NO Oxidation

The reaction orders of NO oxidation were calculated by using the initial rate method. Under different NO concentrations, the initial reaction rates of NO oxidation were calculated as Eq. (27) and the reaction orders of NO (m) were obtained according to Eqs. (28)-(29). The results are shown in Fig. 9, the slope was the reaction order. After fitting, the value of m was 1.04775 (R^2 was

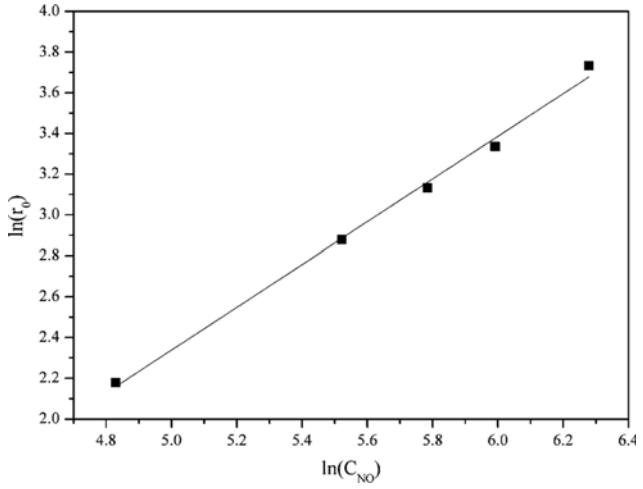

Fig. 9. Reaction orders of NO removal. Gas flow rate: 1.5 L/min, C(O_2)=7%, GHSV: 45,000 h^{-1}, H_2O_2 concentration 2 mol/L, H_2O_2 feeding rate: 5 mL/h, flue gas temperature: 140 °C, reaction temperature: 140 °C.

0.99406), which indicated that it conformed to the pseudo-first-order kinetics pattern.

$$r_0 = -\frac{dC_0}{dt} \tag{27}$$

$$-\frac{dC_0}{dt} = kC_0^m \tag{28}$$

$$\ln\left(-\frac{dC_0}{dt}\right) = \ln(k) + m\ln(C_0) \tag{29}$$

where C is the instantaneous concentration of NO, mg/m^3; t is the reaction time, s; r_0 is the initial reaction rate of NO, mg·m^{-3}·s^{-1}; C_0 is the initial concentration of NO, mg/m^3; k is the reaction rate constant, m^{3-m}·mg^{-m}·s^{-1}; and m is the reaction order.

After the reaction order was determined, Eq. (28) could be further simplified and the logarithm on both sides was taken to obtain Eq. (30). Fig. 10(a) shows the pseudo-first-order reaction rate constants of NO oxidation under different reaction temperatures, which were calculated by using Eq. (30). When the reaction temperature increased from 120 °C to 160 °C, the reaction rate constants for NO were 0.0054 s^{-1}, 0.01163 s^{-1}, and 0.0147 s^{-1}, respectively. It is obvious that the ln k decreases linearly with 1/T, which is fitted to the Arrhenius Equation (Eq. (8)).

$$\ln\left(\frac{C_t}{C_0}\right) = -kt \tag{30}$$

$$\ln(k) = \ln(A) - \frac{E}{R}\times\frac{1}{T} \tag{31}$$

Then the log type was deduced as Eq. (31) and the results presented in Fig. 10(b). The obtained apparent activation energy was 35.72 kJ/mol for NO, which was lower than 42.5 kJ/mol for NO reported by Guo [39]. It was due to the increasing contact area in the gas phase, resulting in a decrease of reaction barrier. Additionally, that of NO using vaporized H_2O_2/$Na_2S_2O_8$ solution was 27.8 kJ/mol in Zhao's report [40], which was lower than our work. It was mainly because the •OH radicals were limited by the gas-solid mass transfer rate. To improve the mass transfer rate and increase effective reactive surface sites, iron-based material with a porous structure might be approached. According to Doyle [27], iron-based catalyst with Al_2O_3 and SiO_2 as supporter showed a stoichiometric efficiency and that was 50-80 times higher than that of the iron oxides. Researches on catalyst are in process and relevant results will be presented in the future.

CONCLUSIONS

In the bench-scale setup, experiments were systematically carried out to investigate the performance of the proposed NO removal system. HPLC and isopropanol injection experiments showed that the •OH radicals were the key to enhancing the NO removal using heterogeneous Fenton reaction. When the NO concentration was 530 ppm and the O_2 concentration was 7%, the NO removal efficiency was 78% under the operation condition where the gas flow rate was 1.5 L/min, flue gas temperature was 140 °C, reaction temperature was 140 °C, GHSV was 45,000 h^{-1}, H_2O_2

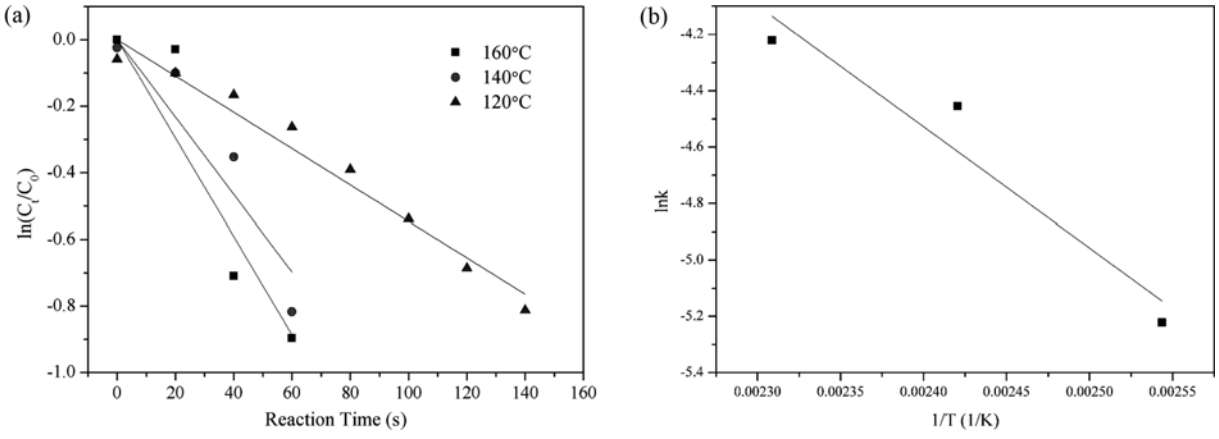

Fig. 10. Determination of apparent activation energies. (a) Reaction rate constants of NO oxidation in different reaction temperatures. (b) Apparent activation energies of NO oxidation.

concentration was 2 mol/L, H_2O_2 feeding rate was 5 mL/h, the ammonium-based absorbent was 5 wt% urea, 5 wt% ammonium sulfite and 0.015 wt% triethanolamine. The ferric nitrate in the reacted catalyst was detected by FTIR spectrogram. The SEM analysis indicated that the aggregation between particles emerged with the experiments going on. From EDX analysis, it was deduced that the corrosion occurred on the surface of catalyst. The analysis of nitrate nitrogen in the aqueous solution showed that the major absorption mechanism of nitrogen oxides, nitrate acid and nitrite acid in the liquid phase was a reduction process. The reaction orders for NO oxidation were determined as 1.04775, and the apparent activation energies were 35.72 kJ/mol. Our future work is to focus on the effects of coexistence gases in flue gas (O_2, SO_2, CO_2) on the NO removal efficiency at various operation conditions and the evolution rule of catalyst in the simultaneous desulfurization and denitrification process. Relevant results will be reported in the future.

ACKNOWLEDGEMENTS

The financial support provided by the National Natural Science Foundation of China (Grant No. 51376047) is appreciated. The authors gratefully acknowledge the students and professor for their helpful comments and valuable suggestions.

SUPPORTING INFORMATION

Additional information as noted in the text. This information is available via the Internet at http://www.springer.com/chemistry/journal/11814.

REFERENCES

1. Y. Jia, D. Du, X. Zhang, X. Ding and O. Zhong, *Korean J. Chem. Eng.*, **30**, 1735 (2013).
2. D. S. Jin, B. R. Deshwal, Y. S. Park and H. K. Lee, *J. Hazard. Mater.*, **135**, 412 (2006).
3. Y. Zhao, F. Liu, T. Guo and Y. Zhao, *Science in China Series E: Technological Sciences*, **52**, 1768 (2009).
4. Y. Liu, J. Zhang, C. Sheng, Y. Zhang and L. Zhao, *Chem. Eng. J.*, **162**, 1006 (2010).
5. J. Zhang, R. Zhang, X. Chen, M. Tong, W. Kang, S. Guo, Y. Zhou and J. Lu, *Ind. Eng. Chem. Res.*, **53**, 6450 (2014).
6. Y. Zhao, Y. Han, T. Guo and T. Ma, *Energy*, **67**, 652 (2014).
7. H. W. Park, S. Choi and D. W. Park, *J. Hazard. Mater.*, **285**, 117 (2015).
8. Y. Zhao, R. Hao and M. Qi, *Chem. Eng. J.*, **269**, 159 (2015).
9. Y. Zhao, R.-L. Hao, Q. Guo and Y.-N. Feng, *Fuel Process. Technol.*, **137**, 8 (2015).
10. E. Sada, H. Kumazawa, I. Kudo and T. Kondo, *Chem. Eng. Sci.*, **33**, 315 (1978).
11. H. Chu, T.-W. Chien and S. Li, *Sci. Total Environ.*, **275**, 127 (2001).
12. J. Wei, Y. Luo, P. Yu, B. Cai and H. Tan, *J. Ind. Eng. Chem.*, **15**, 16 (2009).
13. H. Fennv and Z. Qin, *Environm. Pollution Control*, **5**, 004 (2012).
14. P. Fang, C.-p. Cen, X.-m. Wang, Z.-j. Tang, Z.-x. Tang and D.-s. Chen, *Fuel Process. Technol.*, **106**, 645 (2013).
15. L. Chung and H. S. Huang, Phoenix-nasa low temperature multi-pollutant (no x, so x & mercury) control system for fossil fuel combustion, *Challenges of power engineering and environment*, Springer, 710 (2007).
16. S. Rahim Pouran, A. A. Abdul Raman and W. M. A. Wan Daud, *J. Cleaner Production*, **64**, 24 (2014).
17. M. C. Pereira, L C. A. Oliveira and E. Murad, *Clay Minerals*, **47**, 285 (2012).
18. J. Ding, Q. Zhong and S. Zhang, *J. Mole. Catal. A: Chem.*, **393**, 222 (2014).
19. J. Ding, Q. Zhong, S. Zhang, F. Song and Y. Bu, *Chem. Eng. J.*, **243**, 176 (2014).
20. J. Ding, Q. Zhong, S. Zhang and W. Cai, *J. Hazard. Mater.*, **283**, 633 (2015).
21. X. Huang, J. Ding and Q. Zhong, *Appl. Surf. Sci.*, **326**, 66 (2015).
22. Y. Liu, J. Zhang, J. Pan and A. Tang, *Energy Fuels*, **26**, 5430 (2012).
23. Y. Liu, J. Zhang and Z. Wang, *Chem. Eng. J.*, **197**, 468 (2012).
24. Y. Liu, J. Zhang and Y. Yin, *AIChE J.*, **61**, 1322 (2015).
25. Y. Lu, Y. Xiong and M. Gao, *Proceedings of the CSEE*, **28**, 44 (2008).
26. W. P. Kwan and B. M. Voelker, *Environ. Sci. Technol.*, **37**, 1150 (2003).
27. A. L.-T. Pham, C. Lee, F. M. Doyle and D. L. Sedlak, *Environ. Sci. Technol.*, **43**, 8930 (2009).
28. C. M. Lousada and M. Jonsson, *J. Phys. Chem. C*, **114**, 11202 (2010).
29. L. Milne, I. Stewart and D. H. Bremner, *Ultrasonics Sonochemistry*, **20**, 984 (2013).
30. J L. Rendon and C. J. Serna, *Clay Miner*, **16**, 375 (1981).
31. E. Wolska, *Zeitschrift für Kristallographie-Crystalline Materials*, **154**, 69 (1981).
32. C. X. Gao, Q. F. Liu and D. S. Xue, *J. Mater. Sci. Lett.*, **21**, 1781 (2002).
33. D. A. N. Li, X. Wang, G. Xiong, L. Lu, X. Yang and X. I. N. Wang, *J. Mater. Sci. Lett.*, **16**, 493 (1997).
34. Q. Zhang, I. Lee, J. B. Joo, F. Zaera and Y. Yin, *Acc. Chem. Res.*, **46**, 1816 (2013).
35. R.-t. Guo, J.-k. Hao, W.-g. Pan and Y.-l. Yu, *Sep. Sci. Technol.*, (2014).
36. Y. Zhao, X. Wen, T. Guo and J. Zhou, *Fuel Process. Technol.*, **128**, 54 (2014).
37. P. Fang, C. Cen, Z. Tang, P. Zhong, D. Chen and Z. Chen, *Chem. Eng. J.*, **168**, 52 (2011).
38. Q. Dawei, Z. Jichao, G. Menglong and X. Yuanquan, *Proceedings of the CSEE* (2013).
39. T. X. Guo, Experimental investigation on simultaneous removal of so 2 and no x in liquid phase by new-type complex absorbent, *J. North China Electr. Power Univ.*, 69 (2011).
40. Y. Zhao, R. Hao, P. Zhang and S. Zhou, *Energy Fuels*, **28**, 6502 (2014).

Supporting Information

Enhancement of NO absorption in ammonium-based solution using heterogeneous Fenton reaction at low H_2O_2 consumption

Bo Wu, Yuanquan Xiong†, Jinbo Ru, and Hao Feng

Key Laboratory of Energy Thermal Conversion and Control of Ministry of Education,
School of Energy and Environment, Southeast University, Nanjing 210096, Jiangsu, China
(*Received 7 February 2016 • accepted 2 July 2016*)

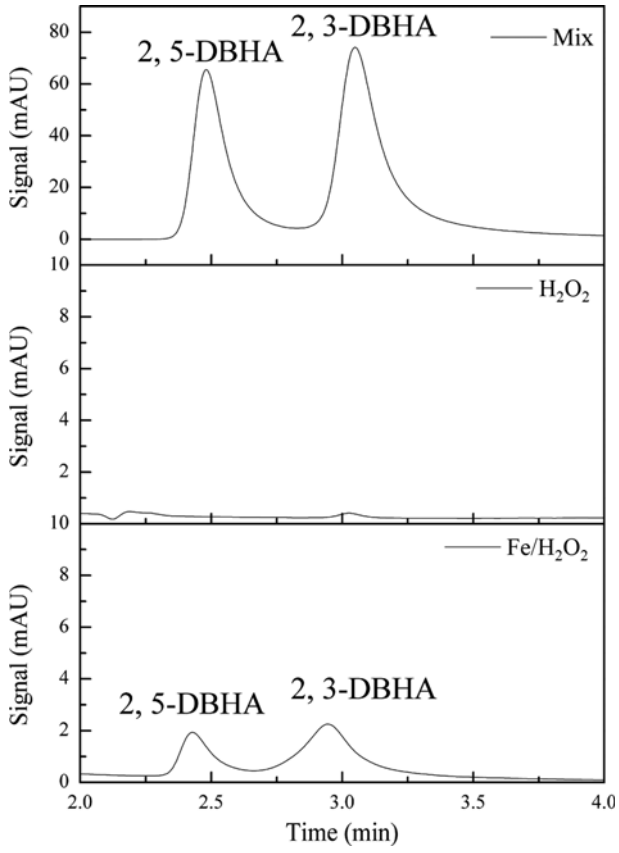

Fig. S1. The HPLC profile for detecting hydroxyl free radicals.

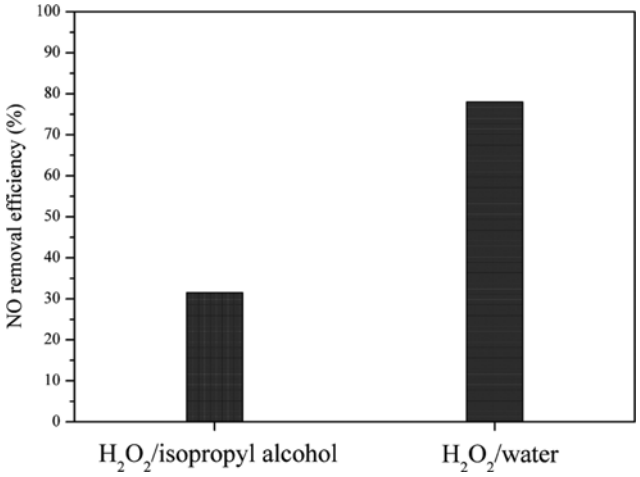

Fig. S2. The isopropanol injection experiments. Conditions: gas flow rate: 1.5 L/min, C(NO)=530 ppm, C(O_2)=7%, flue temperature: 140 °C, reaction temperature: 140 °C, H_2O_2 concentration: 2 moL/L, H_2O0 feeding rate: 5 mL/h, GHSV: 45,000 h^{-1}.